Astrometry via close approach events: applications to main-belt asteroid (702) Alauda

B. F. Guo, Q. Y. Peng, A. Vienne, X. Q. Fang

Monthly Notices of the ROYAL ASTRONOMICAL SOCIETY

MNRAS **525,** 2961–2971 (2023) https://doi.org/10.1093/mnras/stad2454
Advance Access publication 2023 August 17

Astrometry via close approach events: applications to main-belt asteroid (702) Alauda

B. F. Guo,[1,3] Q. Y. Peng,[1,3]★ A. Vienne[2,3] and X. Q. Fang[1,3]

[1]*Department of Computer Science, Jinan University, Guangzhou 510632, China*
[2]*IMCCE, Observatoire de Paris, PSL Research University, CNRS, Sorbonne Université, Université de Lille, Paris F-75014, France*
[3]*Sino-French Joint Laboratory for Astrometry, Dynamics and Space Science, Jinan University, Guangzhou 510632, China*

Accepted 2023 August 9. Received 2023 August 6; in original form 2023 July 12

ABSTRACT

The release of *Gaia* catalogue is revolutionary to the astronomy of Solar system objects. After some effects such as atmospheric refraction and CCD geometric distortion have been taken into account, the astrometric precision for ground-based telescopes can reach the level of tens of milli-arcseconds (mas). If an object approaches a reference star in a small relative angular distance (less than 100 arcsec), which is called close approach event in this work, the relative positional precision between the object and reference star will be further improved since the systematic effects of atmospheric turbulence and local telescope optics can be reduced. To obtain the precise position of a main-belt asteroid in an close approach event, a second-order angular velocity model with time is supposed in the sky plane. By fitting the relationship between the relative angular distance and observed time, we can derive the time of maximum approximation and calculate the corresponding position of the asteroid. In practice, five nights' CCD observations including 15 close approach events of main-belt asteroid (702) Alauda are taken for testing by the 1 m telescope at Yunnan Observatory, China. Compared with conventional solutions, our results show that the positional precision significantly improves, which reaches better than 4 mas, and 1 mas in the best case when referenced for the Jet Propulsion Laboratory (JPL) ephemeris in both right ascension and declination.

Key words: methods: data analysis – techniques: image processing – astrometry – minor planets, asteroids: general.

1 INTRODUCTION

The astrometry of asteroids is helpful to reveal the formation and evolution of the Solar system. For example, the precise positions of asteroids are essential to estimate their accurate orbits (Milani & Gronchi 2010; Desmars et al. 2013). The study of Yarkovsky effect also needs accurate positions of the asteroids (Del Vigna et al. 2018; Greenberg et al. 2020). In addition, the astrometry of asteroids are meaningful to the defense of impact. Spoto et al. (2017) presented that astrometric accuracy affected the impact monitoring of near-Earth asteroids (NEAs), especially for short-arc orbital solutions. Siltala & Granvik (2020) found that the high-accuracy astrometry of an asteroid could reduce the uncertainty of mass estimate.

At present, most observations of asteroids are obtained via ground-based telescopes. The event of stellar occultation is one of the approaches to obtain not only the size and shape of an asteroid, but also the accurate astrometry (Ferreira et al. 2022). For a main-belt asteroid (MBA), a well-observed stellar occultation under the right circumstances can establish the position of the shadow better than 1 km, which is equivalent to less than 0.5 mas (Herald et al. 2020). However, if a stellar occultation by a given asteroid cannot be observed, one may obtain accurate astrometry from close approach events with *Gaia* stars, as described in this work. *Gaia* catalogue (Gaia Collaboration 2023) provides the accurate and precise positions of reference stars, which is revolutionary to the astrometry of Solar system objects. None the less, it is not easy to obtain the accurate and precise positions of asteroids. For a fast-moving asteroid, long trails exist even if a short exposure time is adopted, which causes the loss of precision. Shao et al. (2014) developed the technique of synthetic tracking to obtain accurate positions for NEAs. Later, Zhai et al. (2018) reported the precision can reach the level of 10 mas using this technique. Moreover, the CCD distortion influences the astrometry of asteroids (Peng et al. 2012; Wang et al. 2015), which should be also taken account. In addition, the effect of differential colour refraction (DCR) results in systematic positional errors towards zenith, which should be considered to obtain the accurate and precise positions (Anderson et al. 2006; Velasco et al. 2016).

If we consider the effects of atmospheric turbulence and local telescope optics, the precision of astrometry will be further improved. An asteroid approaches a reference star in a small angular distance (usually less than 100 arcsec), which is called an approach event in this work, during which these effects can be reduced. Similar to close approach event, appulse is also an event with the minimum apparent angular distance between two objects. One of the differences is that the two objects have even smaller angular distance during an appulse so that the extended part of the body (such as the atmosphere) is occulted as shown in Kammer et al. (2020). Another difference is that observations with less spans of angular distances are required (e.g. within the range of only several arcseconds) in an appulse like stellar occultations. The reasons for positional precision improvement in a

★ E-mail: tpengqy@jnu.edu.cn

Table 1. The specifications of CCDs used of the 1m telescope.

Parameter	CCD#1	CCD#2
Size of CCD array	2048 × 2048	4096 × 4112
Size of pixel	13.5 μ × 13.5 μ	15 μ × 15 μ
Approximate scale factor	0.209 arcsec pixel^{-1}	0.233 arcsec pixel^{-1}
Field of view	7.1 arcmin × 7.1 arcmin	16.0 arcmin × 16.0 arcmin
Nights observed	2	3

Table 2. The observations of Alauda overview. The first column shows the observation date. The second column shows the number of frames acquired. The third column shows the exposure time. The fourth column shows the CCD used. The fifth column shows the approximate number of matched *Gaia* stars in the field of view for astrometric calibration. The mean seeings of each night are shown in the sixth column and the last column shows the number of close approach events.

Date (UT)	Frames (no.)	ExpTime (s)	CCD used	Calibrated stars (no.)	Seeing (arcsec)	Approach events (no.)
2020-11-11	242	40	CCD#1	190	3.3	2
2020-11-12	340	30	CCD#1	170	3.2	3
2020-12-08	173	40	CCD#2	860	1.7	4
2021-01-15	130	60	CCD#2	600	1.2	3
2021-02-10	207	60	CCD#2	500	1.2	4

close approach event mainly come from the local similar atmospheric turbulence and telescope optical effect. Morgado et al. (2016) used this method to determine the positional difference between two concerned planetary satellites. This method was successfully applied to the observations of Galilean satellites of Jupiter (Morgado et al. 2019) and satellites of Uranus (Santos-Filho et al. 2019). For the practice of Galilean satellites, the average internal precision can reach 11.3 mas within the angular distance of 30 arcsec (Morgado et al. 2019), which is almost comparable to the positional precision from mutual phenomenon. Lin et al. (2019) found that precision premium occurred within the angular distance of 100 arcsec and the improvement of the precision could be expressed as a sigmoidal function with the angular distance.

In this paper, we want to obtain higher positional precision of an asteroid after considering the effects of image quality, geometric distortion, atmospheric refraction (including DCR effect), atmospheric turbulence, and local telescope optics. Meanwhile, we want to extend the study of the close approach events from two satellites (Morgado et al. 2016, 2019) to an asteroid with respect to its nearby reference star. In fact, the close approach event happens on all the Solar system objects. In this work, considering the aperture size of the telescope used and the available observation time, we choose the typical objects MBAs for testing because of the high signal-to-noise ratios (SNRs), large angular velocity but less trailing. The main-belt asteroid (702) Alauda is appropriate for testing due to the enough calibrated stars in the field of view and several close approach events during one night (also see Section 2).

The remainder of this paper is organized as follows. Section 2 will introduce the telescope, CCDs, and observations. Section 3 will elaborate the reduction method for a main-belt asteroid in a close approach event. Section 4 will show the astrometric reduction results and analysis of main-belt asteroid (702) Alauda. Finally, the drawn conclusions will be presented in the last section.

2 OBSERVATIONS

Five nights' CCD observations including 15 close approach events of asteroid (702) Alauda are taken by the 1m telescope at Yunnan Observatory, China (IAU code: 286). Totally, 1092 CCD frames are taken from 2020 November 11 to 2021 February 10. We exclude some observations (∼2 per cent of the total) when they are taken with the nearby service lights turned on by mistake. For the telescope used, the diameter of the primary mirror is 101.6 cm, and the *f* ratio is 13.3. Two different CCDs are used during our observation. The specifications of the CCDs are listed in Table 1. As we aimed to minimize the effect of DCR, according to Stone (2002) and Lin, Peng & Zheng (2020), we adopt the scheme that all the observations are taken with *Cousins-I* filter and the observational zenith distances are less than 60°. To ensure the measured positional precision of Alauda, we empirically make its trailing less than 1/3 of seeing. The visual magnitude of Alauda is 12 ∼ 13 during the observation. The magnitude differences between Alauda and nearby reference stars (the visual magnitude of Alauda and *Gaia-G* magnitude of stars) are less than 5. More details of the observations are shown in Table 2.

3 METHOD

3.1 Data reduction

First, all CCD frames are pre-processed by bias and flat-field corrections. Then, for each frame, we detect all the sources and measure their pixel coordinates with two-dimensional Gaussian centring algorithm. Specifically, for each image, one can refer to DAOPHOT program (Stetson 1987) for detecting each source and deriving its initial position in pixel coordinate. To further measure the pixel coordinate of each source, we use the two-dimensional Gaussian centring algorithm. For more details of the centring algorithm, one can refer to equation (3) in Lin et al. (2021). Secondly, we match these sources with the stars in *Gaia* DR3 catalogue (Gaia Collaboration 2023) and calculate their topocentric astrometric positions at the observational epoch. To ensure the precision of calibration, we exclude the stars with their renormalized unit weight errors in *Gaia* catalogue larger than 2.0 (Zheng et al. 2022). In addition, we calibrate the DCR effect of the matched *Gaia* stars and Alauda according to Lin et al. (2020). Thirdly, we calculate the standard coordinate of each matched star through the central projection (Green 1985), and solve the plate model with a weighted fourth order polynomial (Lin et al. 2019), in which some effects such as the geometric distortion

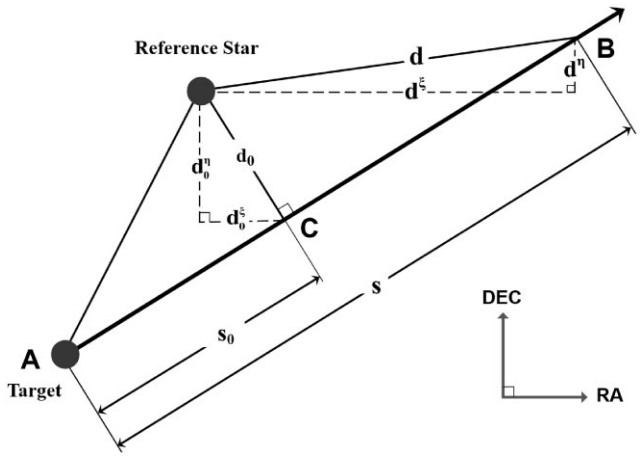

Figure 1. Schematic diagram of the motion model. The target moves relative to a reference star nearby along line *ACB* with its starting point *A* and has its zero recording time ($t = 0$) at the point *A*. The point *C* corresponds the relative minimum angular distance d_0 (also called the impact parameter) between the target and reference star, and has a shift s_0 from the point *A*. d_0^ξ and d_0^η are the projections of d_0 in right ascension and declination, respectively. At any moment of t, the target moves to the point B with the distance d relative to the reference star, and the shift s equals the distance of *AB*. d^ξ and d^η are the projections of d in right ascension and declination, respectively.

and atmospheric refraction can be absorbed. Finally, the observed position (the topocentric astrometric position) of Alauda can be calculated via the solved plate model. Finally, by referring for some ephemeris, the positional ($O - C$; the observed minus computed) of Alauda can be conveniently calculated.

3.2 Close approach model

In Fig. 1, an asteroid (also called target) moves in the sky plane during a close approach event. It is supposed that the angular velocity can be expressed as a second order polynomial with time in the standard coordinate,

$$v = a_0 + a_1 t + a_2 t^2, \tag{1}$$

where v is the angular velocity of the target changing with time, and parameters $a_0 \sim a_2$ are the constants. At any moment of t, the target moves to B with the shift s with respect to the starting point A where its recording time t is zero. During a close approach event, the asteroid has its maximum approximation at point C. The point C corresponds the minimum relative angular distance d_0 (also called the impact parameter) between the target and reference star, and has an offset s_0 from the point A. At the moment of t, the target has a distance d relative to the reference star in the standard coordinate. Thus, d^2 has the following relationship,

$$d^2 = p_0 + p_1 t + p_2 t^2 + p_3 t^3 + p_4 t^4 + p_5 t^5 + p_6 t^6. \tag{2}$$

Similar to Morgado et al. (2019), we can fit the square of distance d^2 in equation (2) by the weighted least squares scheme for this sixth order polynomial with seven parameters ($p_0 \sim p_6$). Here, the weighted scheme is used according to the sigmoidal function (precision premium curve) as shown in Lin et al. (2019). The observed positions (which are calculated in Section 3.1) of the target and reference star in each frame are used to calculate d^2 and for fitting. The fitted curve is also called distance curve in Morgado et al. (2019). At the central instant t_0, the target has its impact parameter d_0, which can be computed by differentiating equation (2) and let it zero. Then, the expression will be shown as the following equation,

$$p_1 + 2p_2 t_0 + 3p_3 t_0^2 + 4p_4 t_0^3 + 5p_5 t_0^4 + 6p_6 t_0^5 = 0, \tag{3}$$

where t_0 comes from the determination of the root in equation (3). Based on Newton–Raphson method, we can conveniently solve the value of t_0 via programming. Then, we can calculate the impact parameter d_0 ($d_0 = d$ at the moment of t_0) according to the solved t_0 and parameters $p_0 \sim p_6$.

3.3 Calculate the (O − C) in a close approach event

In Fig. 1, the motion of the target in the standard coordinate can be decomposed in right ascension (RA) and declination (Dec.). In each direction, we can also respectively fit the square of component distance $(d^\xi)^2$ and $(d^\eta)^2$ by a sixth order polynomial with time [i.e. equation (2)]. Then, we substitute the central instant t_0, which corresponds to the resultant minimum distance d_0 (which is solved in Section 3.2), to the respective fitted sixth order polynomial in each direction. Thus, we can conveniently calculate the components of the minimum distance (impact parameter) d_0^ξ in RA and d_0^η in Dec. in the standard coordinate. For the positions of the reference star, we can calculate its mean observed position ($\xi^{\rm R}$, $\eta^{\rm R}$) (the superscript R stands for the reference star) in the same standard coordinate. Of course, we can also directly use the computed position based on the catalogue (if the catalogue provides the precise position of the reference star). Then, the observed position of the target ($\xi_{\rm o}^{\rm T}$, $\eta_{\rm o}^{\rm T}$) (the superscript T stands for the target, while the subscript O stands for the observed position) at the moment of t_0 can be expressed as,

$$\begin{cases} \xi_{\rm o}^{\rm T} = \xi^{\rm R} + d_0^\xi \\ \eta_{\rm o}^{\rm T} = \eta^{\rm R} + d_0^\eta \end{cases}. \tag{4}$$

The signs (positive or negative) of d_0^ξ and d_0^η should be determined according to the relative position between the target and reference star by the observation near the moment of t_0. Through reprojection (Green 1985), we can calculate the observed position of the target ($\alpha_{\rm o}^{\rm T}$, $\delta_{\rm o}^{\rm T}$) in equatorial coordinate. We can acquire the computed position of the target ($\alpha_{\rm c}^{\rm T}$, $\delta_{\rm c}^{\rm T}$) from some ephemeris by submitting the central instant t_0. Finally, we can calculate the positional ($O - C$) (the observed minus computed) of the target in a close approach event.

3.4 Comparison with previous works

Although our reduction method of close approach event is somewhat similar to Morgado et al. (2016, 2019), there are still some differences. The major difference is the coordinate system used during the reduction process. They reduced the observations in pixel coordinate, which introduces some problems: the determination of pixel scale, the orientation of CCD, and geometric distortion. In this work, we reduce the observations in standard coordinate (the projection of equatorial coordinate), in which these effects can be calibrated in the plate model. In addition, we extend the method from two Galilean moons to a main-belt asteroid and its nearby reference star. Morgado et al. (2016, 2019) supposed the angular velocity with a first order polynomial with time and fitted the distance curve [equation (2)] with a fourth order polynomial, while we suppose the angular velocity with a second order polynomial and fit the distance curve with a sixth order polynomial to better reflect the accuracy and precision in the practice of a main-belt asteroid, which will be further discussed in Section 4.

Table 3. The reduced results for all the used observations of main-belt asteroid (702) Alauda. The second column shows the *Gaia* IDs of the reference stars for each close approach event. The third column gives the central instants (t_0) in form of JD-2459000. The fourth and fifth columns list the ($O - C$)s of Alauda in RA and Dec., which are derived from the fitted scheme of both 4th order and 6th order polynomials, respectively. The impact parameters and magnitudes of the reference stars (*Gaia-G* magnitude) are listed in the sixth and seventh columns, respectively. The eighth column shows the estimated uncertainty of central instant according to Morgado et al. (2016). The ninth and tenth columns respectively show the observed minimum and maximum angular distance between Alauda and the reference star. The last column shows the duration for each close approach event. Below the results of each observation set, the mean positional ($O - C$)s and standard deviations are also listed together with conventional solutions.

Date (UT)	Reference star ID	t_0 (JD-2459000)	$\Delta\alpha\cos\delta$ (arcsec) 6th order (4th order)	$\Delta\delta$ (arcsec) 6th order (4th order)	d_0 (arcsec)	Star mag	σ_{t_0} (s)	Min dis (arcsec)	Max dis (arcsec)	Duration (h)
2020-11-11	190965107955867776	165.3385796	−0.003 (−0.003)	0.001 (−0.002)	7.81	14.2	0.784	7.81	60.85	2.80
2020-11-11	190965103659693952	165.3713975	0.003 (0.006)	−0.001 (−0.002)	14.68	13.8	0.938	14.68	36.09	2.80
2020-11-12	190945110588179456	166.3279130	0.004 (0.007)	−0.004 (−0.002)	33.09	15.3	1.682	33.08	57.61	3.05
2020-11-12	190945106293176064	166.3411577	0.000 (−0.001)	−0.004 (−0.003)	19.22	16.2	3.125	19.23	44.57	3.05
2020-11-12	190945316746612608	166.3598021	0.004 (−0.007)	−0.001 (−0.001)	24.57	15.4	1.282	24.58	41.48	3.05
–	–	Average position (4th order)	0.001 ± 0.006	−0.002 ± 0.001	–	–	–	–	–	–
–	–	Average position (6th order)	0.001 ± 0.003	−0.002 ± 0.002	–	–	–	–	–	–
–	–	Conventional solution	0.006 ± 0.010	−0.002 ± 0.008	–	–	–	–	–	–
2020-12-08	188197534110556032	192.1526737	0.004 (0.005)	0.004 (0.002)	30.94	16.0	2.322	30.93	70.54	2.44
2020-12-08	188197534110557952	192.1595573	−0.002 (−0.009)	−0.002 (−0.001)	23.43	15.0	0.988	23.42	62.34	2.44
2020-12-08	188197534110557696	192.1675330	0.004 (0.002)	−0.002 (−0.001)	38.02	15.4	1.422	38.02	63.85	2.44
–	–	Average position (4th order)	−0.002 ± 0.007	0.000 ± 0.002	–	–	–	–	–	–
–	–	Average position (6th order)	0.002 ± 0.003	0.000 ± 0.003	–	–	–	–	–	–
–	–	Conventional solution	−0.001 ± 0.012	−0.001 ± 0.008	–	–	–	–	–	–
2021-01-15	173523550707799552	230.0214632	−0.003 (0.002)	−0.011 (−0.006)	15.17	16.7	1.454	15.15	43.50	2.54
2021-01-15	173523275829562624	230.0590659	−0.005 (−0.008)	−0.014 (−0.006)	72.65	13.8	2.245	72.65	82.44	2.54
2021-01-15	173523344549362432	230.0668542	0.000 (−0.003)	−0.006 (−0.005)	32.20	15.6	1.355	32.21	54.01	2.54
–	–	Average position (4th order)	−0.003 ± 0.005	−0.006 ± 0.001	–	–	–	–	–	–
–	–	Average position (6th order)	−0.003 ± 0.003	−0.010 ± 0.004	–	–	–	–	–	–
–	–	Conventional solution	−0.001 ± 0.007	−0.005 ± 0.009	–	–	–	–	–	–
2021-02-10	159439940627025408	256.0220522	0.000 (0.003)	0.001 (0.000)	47.25	12.1	3.426	47.24	76.93	4.27
2021-02-10	159440048001339008	256.0370666	−0.001 (0.000)	−0.002 (−0.002)	27.49	15.4	1.720	27.48	60.72	4.27
2021-02-10	159439910562389760	256.0984256	0.000 (0.004)	−0.003 (−0.003)	53.03	14.7	1.832	53.03	69.98	4.27
2021-02-10	159439738763696640	256.1304893	−0.002 (−0.001)	0.000 (−0.003)	25.45	16.0	2.162	25.44	64.39	4.27
–	–	Average position (4th order)	0.001 ± 0.002	−0.002 ± 0.002	–	–	–	–	–	–
–	–	Average position (6th order)	−0.001 ± 0.001	−0.001 ± 0.001	–	–	–	–	–	–
–	–	Conventional solution	0.001 ± 0.007	−0.003 ± 0.010	–	–	–	–	–	–

4 RESULTS

4.1 Astrometric results

As shown in Section 3.1, we calculate the positional ($O - C$)s of Alauda in each frame, which are here called the conventional solutions. The observed positions (as calculated in Section 3.1) in each frame are further used for calculation and fitting to derive the observed positions of each close approach event. For this astrometric reduction, the positional effects of geometric distortion, atmospheric refraction, DCR effect have been taken into account. In addition, we notice that there is a satellite of Alauda, which might affect our positional measurement. According to light ratio, mass ratio, and the angular distance between the primary and its satellite presented in Rojo & Margot (2011), the evaluated positional difference between their photocentre and the centre of mass caused by the satellite is less than negligible 1 mas using the method of Peng et al. (2023).

In order to derive the positional ($O - C$) of Alauda for each close approach event (at the moment of maximum approximation), we compute the square of the observed distance d^2 between the target and reference star in the standard coordinate. Then, we can solve the central instant t_0 by solving the root of equation (3). Meanwhile, we also fit the six order polynomials [equation (2)] in the direction of RA and Dec.. Based on the solved central instant t_0, we can calculate the component of the minimum distance d_0^ξ in RA and d_0^η in Dec.. According to equation (4), we calculate the observed positions of the target and project it to the equatorial coordinate. The computed positions of the target are derived from the Jet Propulsion Laboratory (JPL) ephemeris (JPL#116 and DE441). For comparison, we also calculate the results if supposing the squares of the relative distances [d^2, $(d^\xi)^2$, $(d^\eta)^2$] are the fourth order polynomials with time. The results of the positional ($O - C$) are shown in Table 3 together with some information of each close approach event.

Compared with conventional solutions, the positional precision of results from close approach events (fitted with both fourth and sixth order polynomial) are improved significantly. The observed topocentric astrometric positions of Alauda (fitted by six order polynomials) via close approach events are shown in Table 4. For the scheme of fitted by a fourth order polynomial, the standard variations of each observation set are 0.002 arcsec ∼ 0.007 arcsec and 0.001 arcsec ∼ 0.002 arcsec in RA and Dec., respectively. For the scheme of fitted by a sixth order polynomial, the standard variations of each observation set are 0.001 arcsec ∼ 0.003 arcsec and

Table 4. The table shows the topocentric astrometric positions of asteroid (702) Alauda via close approach event. The IAU code of the observatory is 286. The first column lists the Julian dates of maximum approximation. The second and third columns list the corresponding positions in right ascension (RA) and declination (Dec.), respectively.

Julian date	RA (h m s)	Dec. (° ′ ″)
2459 165.338 5796	05 36 42.5223	+ 39 46 37.745
2459 165.371 3975	05 36 41.1470	+ 39 46 35.894
2459 166.327 9130	05 36 02.0518	+ 39 45 42.400
2459 166.341 1577	05 36 01.4756	+ 39 45 41.572
2459 166.359 8021	05 36 00.6663	+ 39 45 40.382
2459 192.152 6737	05 12 10.8423	+ 38 29 09.676
2459 192.159 5573	05 12 10.3978	+ 38 29 07.612
2459 192.167 5330	05 12 09.8837	+ 38 29 05.222
2459 230.021 4632	04 41 41.7784	+ 34 02 06.951
2459 230.059 0659	04 41 40.8386	+ 34 01 49.600
2459 230.066 8542	04 41 40.6437	+ 34 01 45.992
2459 256.022 0522	04 40 31.0515	+ 31 00 06.122
2459 256.037 0666	04 40 31.2851	+ 31 00 00.680
2459 256.098 4256	04 40 32.2478	+ 30 59 38.324
2459 256.130 4893	04 40 32.7584	+ 30 59 26.573

0.001 arcsec $\sim$ 0.004 arcsec in RA and Dec., respectively. Both the mean $(O - C)$s from close approach events are similar to the results of conventional solutions. In our observations, the angular velocity of the target in RA usually strides across the peak of the velocity variation caused by diurnal parallax, while the angular velocity in Dec. is not. Considering the effect of diurnal parallax, we adopt the scheme of fitting by a sixth order polynomial, which will better reflect the accuracy and precision in the practice. Usually for a main-belt asteroid, if we observe the target within a short time span (e.g. within 2 h) and the angular velocity will not stride across the peak of the velocity variation, a fourth order polynomial for fitted can derive good results. In Section 4.3, we will present the difference of the fitted residual in a specific case.

With the fitted scheme of a sixth order polynomial, we do not find the obvious relevance between positional accuracy and magnitudes of reference stars or the impact parameters, which can be shown in Fig. 2, because the effects of atmospheric turbulence and local telescope optics might not be dominant in positional errors. The positional accuracy of each event might be also affected by the other conditions such as the uncertainty of central instant. However, we think the dominating effect in this work is the centring errors of Alauda and reference stars, which will be elaborated in the following subsection. In Fig. 2, most of the absolute positional residuals ($\sqrt{(\Delta\alpha\cos\delta)^2 + (\Delta\delta)^2}$) range from 2 to 6 mas, except two in different shape. The positional absolute residual in blue diamond might be affected by the larger impact parameter, while the residual in red asterisk might be due to the faintness of the reference star.

4.2 Case analysis

In this subsection, we will analyse two typical cases for the close approach events in this work. For more details of the close approach events, one can find Fig. A1–A15 of all the distance curves and the fitted residuals with a sixth order polynomial in the Appendix. Fig. 3 shows the fitted residuals of equation (2) with time when Alauda approached the reference star whose *Gaia* ID is 190965103659693952 observed on 2020 November 11. The left-hand panel shows the fitted residuals of resultant d^2, while the right-hand panel shows residuals of the components $(d^\xi)^2$ in RA and $(d^\eta)^2$ in Dec.. The residual dispersion of d^2, $(d^\xi)^2$, and $(d^\eta)^2$ almost show the consistency with time. Near the central instant $t_0 = 0.371$ (with the minimum relative angular distance d_0), the dispersion of fitted residuals reach the minimum, which is mainly due to the similar effects of atmospheric turbulence and local telescope optics when the relative angular distance is small. However, the minimum dispersion may not be exactly located at the moment of t_0 for the possible reasons of the change of seeing, air mass, and the characteristics of local CCD chip. The mentioned factors affect the precision of centring, and further affect the observed d^2 for fitting.

Fig. 4 shows the fitted residuals of d^2 in equation (2) for another close approach event observed on 2021 February 10 with the nearby reference star's *Gaia* ID 159439940627025408. For the left-hand panel, we notice that near the moment of $t_0 = 0.022$, the dispersion of fitted residual for d^2 is small. The dispersion reaches the minimum near the moment of $t = 0.035$. From the right-hand panel, the dispersion of $(d^\xi)^2$ in RA reaches the minimum near the moment of $t = 0.035$, whereas the dispersion $(d^\eta)^2$ in Dec. reaches the minimum near the moment of $t = 0.08$. The reasons are presented as follows. First,

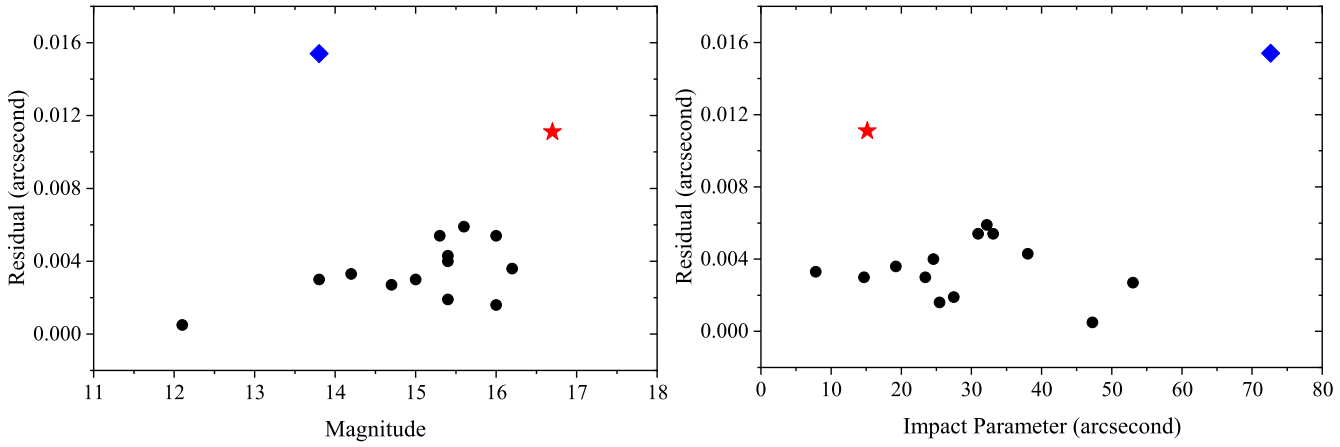

Figure 2. In this figure, the left-hand panel shows the distributions of the absolute positional residuals ($\sqrt{(\Delta\alpha\cos\delta)^2 + (\Delta\delta)^2}$) derived from close approach events against *Gaia-G* magnitudes, while the right-hand panel shows the distributions against impact parameters. The residuals plotted in blue diamond and red asterisk are distinguished for their larger values. The residual in blue diamond is large (left-hand panel) might be due to its large impact factor (right-hand panel). The residual in red asterisk is large (right-hand panel) might be due to the faintness of the reference star (left-hand panel).

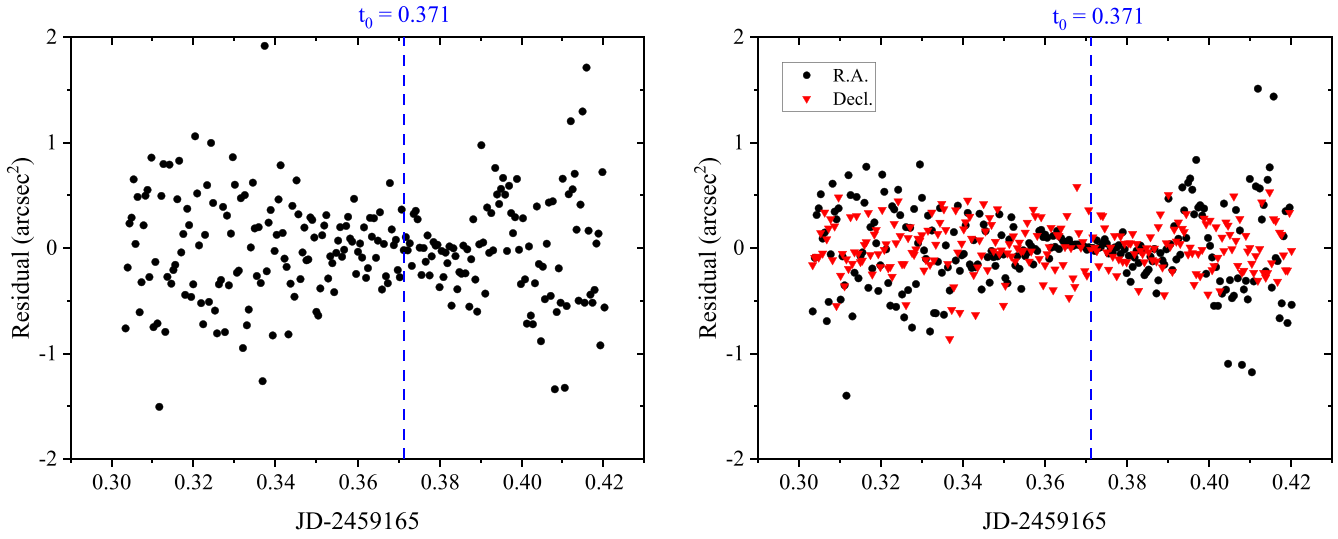

Figure 3. The fitted residuals of d^2 in equation (2) with time in a close approach event observed on 2020 November 11. The *Gaia* ID of the reference star is 19096510365969 3952. The left-hand panel shows the resultant fitted residuals, while the right-hand panel shows the components in the direction of RA and Dec..

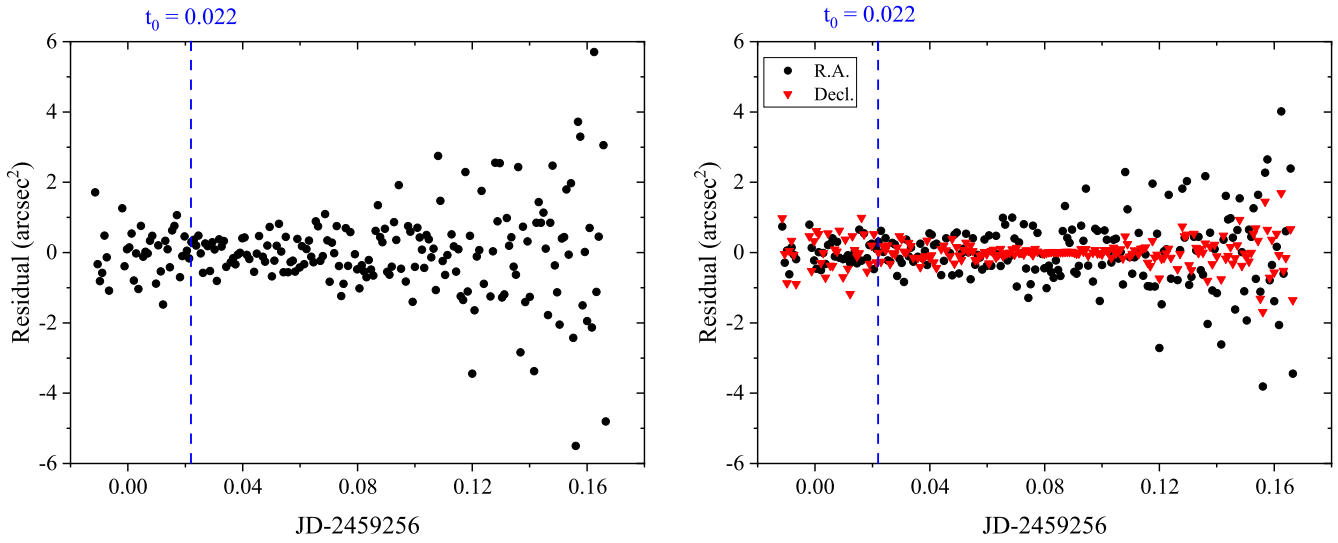

Figure 4. The fitted residuals of d^2 in equation (2) with time in a close approach event observed on 2021 February 10. The *Gaia* ID of the reference star is 159439940627025408. The left-hand panel shows the resultant fitted residuals, while the right-hand panel shows the components in the direction of RA and Dec..

near the moment of $t = 0.08$, the SNRs of the sources in the field of view are higher due to the better weather conditions, and the centring errors of both Alauda and the reference star become smaller. Fig. 5 shows the change of SNRs of both Alauda and the reference star. It can be seen that near the moment of $t = 0.08$, the SNRs of the reference star are larger due to the better weather conditions, which makes the positional precision better. The SNRs of Alauda will be affected by the weather conditions, other nearby stars, and its rotation. Secondly, the telescope used is equatorial-mounted. The tracking accuracy in RA becomes worse when pointing to the west. Hence, the dispersion residuals in the direction of RA and Dec. are not consistent.

Theoretically, in a close approach event, the dispersion of fitted residual of d^2 will reach the minimum with the minimum relative angular distance d_0 at the moment of t_0. However, in fact, the centring errors will be affected by some factors such as the change of weather conditions, air mass, tracking accuracy, dome occlusion, and local characteristics of CCD chip. These effects might affect and dominate the positional errors. If the asteroid with higher SNR approaches brighter reference stars, the positional errors might be dominated by the atmospheric turbulence and local telescope optics. In such a case, we believe that more precise positions will be obtained from close approach events.

4.3 Discussion

In this work, we suppose that the angular velocity of a main-belt asteroid is a second order polynomial with time as shown in equation (1) in a close approach event. Fig. 6 shows the change of angular velocity with time from 2021 November 11 to 2021 November 15 in both RA and Dec. from JPL ephemeris. It can be seen that the angular velocity changes sinusoidally with time due to the diurnal parallax. During the time, the declination of Alauda is about 40° and the amplitudes in both RA and Dec. are numerically similar. For the asteroids (especially for NEAs) in a close approach event, to obtain

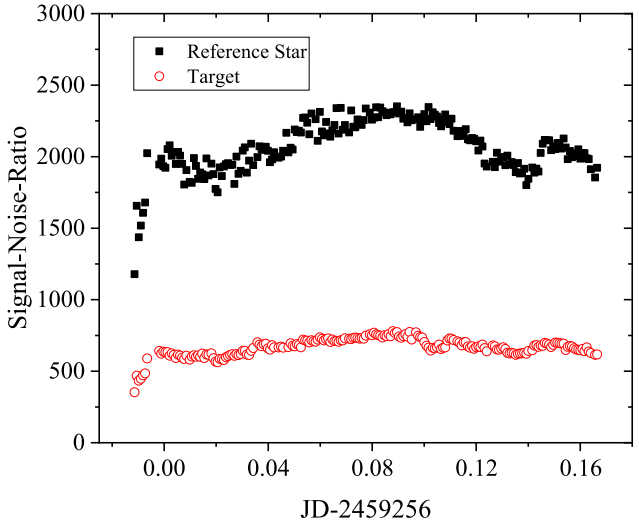

Figure 5. The figure shows the change of SNRs of Alauda and reference star (*Gaia* ID: 1594399406270254 08) with time on 2021 February 10. The red and black spots shows the SNRs of Alauda and the reference star, respectively.

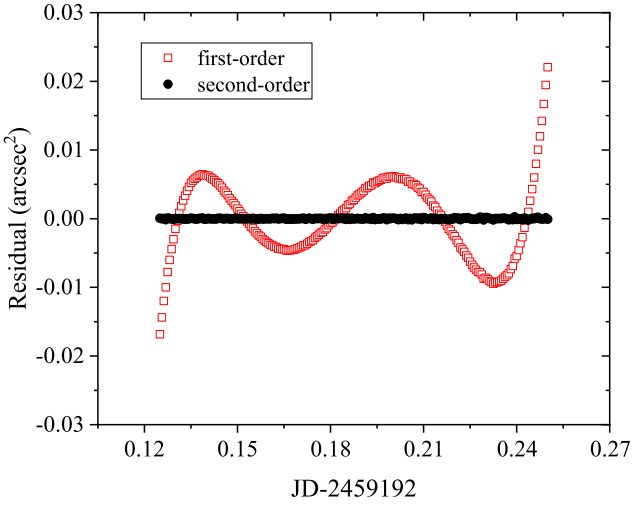

Figure 7. The figure shows the fitted residuals of d^2 with time. The red plots show the fitted residuals with the angular velocity model with a first order polynomial, while the black shows fitted residuals of the angular velocity model with a second order polynomial.

the precise positions with the level of several milli-arcseconds, the angular velocity model of at least the second order polynomial with time should be supposed. For comparison, Fig. 7 shows the fitted residuals of d^2 with different supposed angular velocity models in the close approach event of reference star ID 1881975341105579 52 on 2020 December 8. The positions of Alauda are taken from JPL ephemeris while the position of the star are from *Gaia* DR3 catalogue. The angular velocity model with a second order polynomial (d^2 is a sixth order polynomial with time) can be fitted better with the residuals close to zero. If we take the angular velocity model with a first order polynomial (d^2 is a fourth order polynomial with time), the fitted residuals can reach about 0.2 arcsec^2 (depend on the central instant), which might cause the positional errors of several milli-arcseconds in a close approach event. With the fixed fitted errors, the positional errors depend on the values of impact parameter (d_0, d_0^{ξ}, and d_0^{η}). The smaller the impact parameter is, the larger positional error will cause. The difference of the two fitted velocity models (first-order or second-order polynomial) is the consideration of diurnal parallax effect. We can fit the diurnal parallax effect well using a second-order polynomial velocity model. There will be larger diurnal parallax effect for angular velocities of NEAs. Therefore, we should also consider this effect using the second-order polynomial velocity model for NEAs to derive accurate positions. For Kuiper-belt objects (KBOs), both their angular velocities and diurnal parallax effects are much smaller. The technique in this work might not work well for KBOs because they only pass across the small angular distance during one night. However, if one would like to make use of the close approach event, we still recommend using the second-order polynomial velocity model so that the diurnal parallax effect can be well considered. Perhaps, for the close approach event of natural satellites, the angular velocity model with higher order polynomial with time should be supposed to obtain the precise positions (e.g. with the precision better than 5 mas).

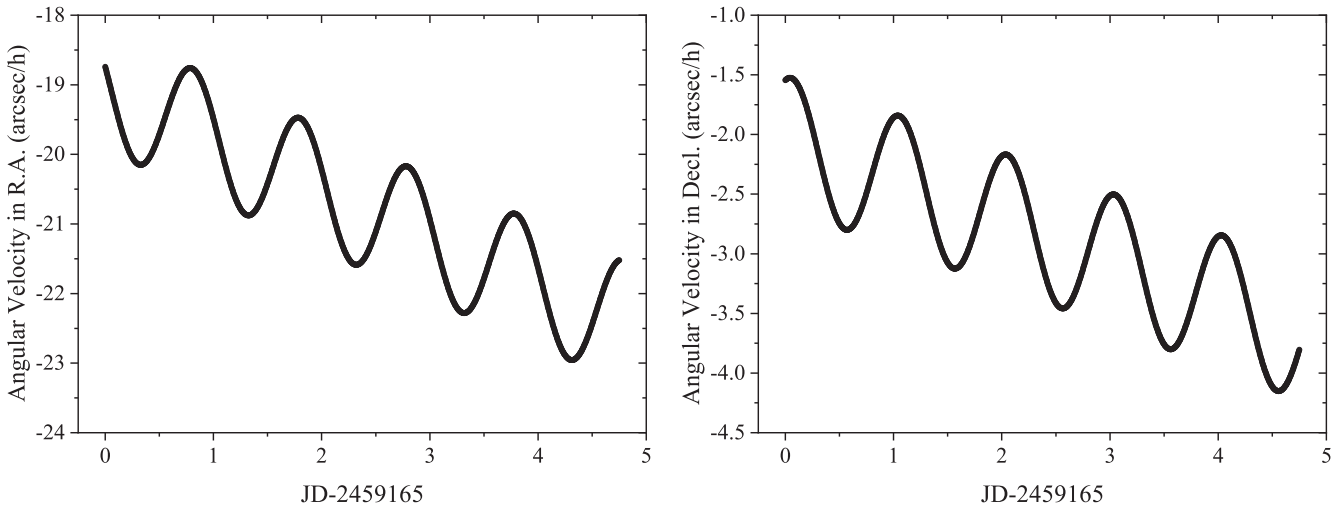

Figure 6. The change of Alauda's angular velocity with time of JD 2459 165 ∼ 2459 169 (2020 November 11 ∼ 2020 November 15) from JPL ephemeris. The left-hand and right-hand panels show the angular velocity with time in RA and Dec., respectively.

The keys to obtaining precise position in this work are presented as follows. First, we reduce the observations in standard coordinate instead of pixel coordinate. In this way, the effects of pixel scale, CCD orientation, geometric distortion, and atmospheric refraction can be taken into account using accurate and precise positions of calibrated stars provided by *Gaia* catalogue. Secondly, the DCR effect of both the target and reference star should be calibrated. These positional systematical errors affect the calculation of the relative angular distance between the target and reference star. Even if we used the *Cousins-I* filter to minimize the DCR effect, the positional errors of relative angular distance might reach about 10 mas for each frame (mainly depend on the observed zenith distance and the different colour indices between the target and reference stars). Thirdly, when the object passes through a dense star field, observations of multiple close approach events can be captured during one night and more precise positions can be obtained. To fully tap the potential of close approach event, the target and nearby reference star should be bright enough so that the effects of atmospheric turbulence and local telescope optics dominate the positional errors.

5 CONCLUSION

In this work, we explore a method to obtain the precise positions of a main-belt asteroid in the close approach event. We perform reduction in the standard coordinate to calibrate the effects of pixel scale, CCD orientation, and geometric distortion. To further improve the fitted precision, the angular velocity model with a second order polynomial is supposed. In practice, 15 close approach events of the main-belt asteroid (702) Alauda are taken over five nights. The positional precision of the close approach events reach 1∼3 and 1∼4 mas in RA, and Dec., respectively. Compared with the similar work of Morgado et al. (2019), we extend the application from Galilean moons to a main-belt asteroid and the reference star nearby. We derive better precision for the asteroid (702) Alauda compared with the precision of 11.3 mas in the practice of Galilean moons. If we tap the potential of the close approach event in the proper conditions, the positional precision might be comparable to that from stellar occultation.

ACKNOWLEDGEMENTS

This work was supported by the National Key R&D Program of China (grant no. 2022YFE0116800), by the China Manned Space Project (grant no. CMS-CSST-2021-B08), by the National Natural Science Foundation of China (grant nos. 11873026, 11273014) and Joint Research Fund in Astronomy (grant no. U1431227). We thank the anonymous reviewer who provided us with valuable comments, Dr Lin F. R. who had a helpful discussion with us and Mr Cao J. L. who helped us match the observations. This work has made use of data from the European Space Agency (ESA) mission Gaia (https://www. cosmos.esa.int/gaia), processed by the Gaia Data Processing and Analysis Consortium (DPAC; hppts://www.cosmos.esa.int /web /gaia/dpac/consortium). Funding for the DPAC has been provided by national institutions, in particular the institutions participating in the Gaia Multilateral Agreement.

DATA AVAILABILITY

The data underlying this article will be shared on reasonable request to the corresponding author.

REFERENCES

Anderson J., Bedin L. R., Piotto G., Yadav R. S., Bellini A., 2006, A&A, 454, 1029
Del Vigna A., Faggioli L., Milani A., Spoto F., Farnocchia D., Carry B., 2018, A&A, 617, A61
Desmars J., Bancelin D., Hestroffer D., Thuillot W., 2013, A&A, 554, A32
Ferreira J. F., Tanga P., Spoto F., Machado P., Herald D., 2022, A&A, 658, A73
Gaia Collaboration, 2023, A&A, 674, A1
Green R. M., ed., 1985, Spherical Astronomy. Cambridge Univ. Press, Cambridge, p. 546
Greenberg A. H., Margot J.-L., Verma A. K., Taylor P. A., Hodge S. E., 2020, AJ, 159, 92
Herald D. et al., 2020, MNRAS, 499, 4570
Kammer J. A. et al., 2020, AJ, 159, 26
Lin F. R., Peng J. H., Zheng Z. J., Peng Q. Y., 2019, MNRAS, 490, 4382
Lin F. R., Peng Q. Y., Zheng Z. J., 2020, MNRAS, 498, 258
Lin F. R., Peng Q. Y., Zheng Z. J., Guo B. F., Shang Y. J., 2021, Ap&SS, 366, 59
Milani A., Gronchi G. F., 2010, Theory of Orbital Determination. Cambridge Univ. Press, Cambridge
Morgado B., Assafin M., Vieira-Martins R., Camargo J. I. B., Dias-Oliveira A., Gomes-Júnior A. R., 2016, MNRAS, 460, 4086
Morgado B. et al., 2019, MNRAS, 482, 5190
Peng Q. Y., Vienne A., Zhang Q. F., Desmars J., Yang C. Y., He H. F., 2012, AJ, 144, 170
Peng Q. Y., Guo B. F., Vienne A., Tian W., Lu X., Zheng Z. J., 2023, A&A, 672, A61
Rojo P., Margot J. L., 2011, ApJ, 727, 69
Santos-Filho S., Assafin M., Morgado B. E., Vieira-Martins R., Camargo J. I. B., Gomes-Júnior A. R., Benedetti-Rossi G., 2019, MNRAS, 490, 3464
Shao M., Nemati B., Zhai C., Turyshev S. G., Sandhu J., Hallinan G., Harding L. K., 2014, ApJ, 782, 1
Siltala L., Granvik M., 2020, A&A, 633, A46
Spoto F. et al., 2017, A&A, 607, A21
Stetson P. B., 1987, PASP, 99, 191
Stone R. C., 2002, PASP, 114, 1070
Velasco S. et al., 2016, MNRAS, 460, 3519
Wang N., Peng Q. Y., Zhang X. L., Zhang Q. F., Li Z., Meng X. H., 2015, MNRAS, 454, 3805
Zhai C. et al., 2018, AJ, 156, 65
Zheng Z. J., Peng Q. Y., Vienne A., Lin F. R., Guo B. F., 2022, A&A, 661, A75

APPENDIX A: DISTANCE CURVE AND FITTED RESIDUAL

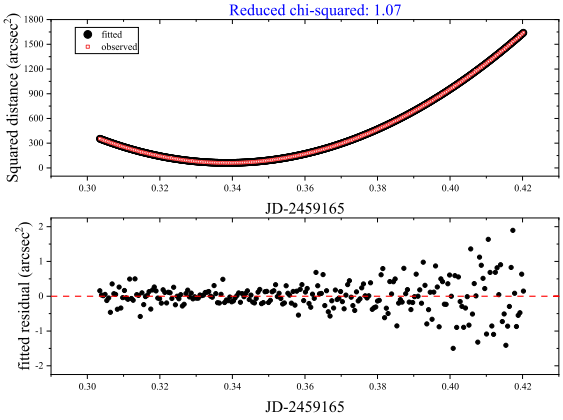

Figure A1. The figure shows the distance curve and fitted residuals of d^2 with time. The reference star ID is 190965107955867776, approached on 2020 November 11.

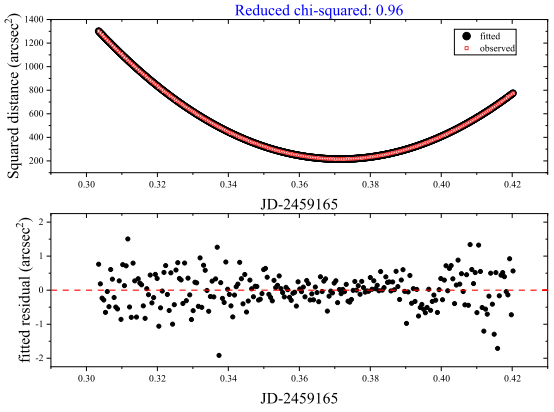

Figure A2. The figure shows the distance curve and fitted residuals of d^2 with time. The reference star ID is 190965103659693952, approached on 2020 November 11.

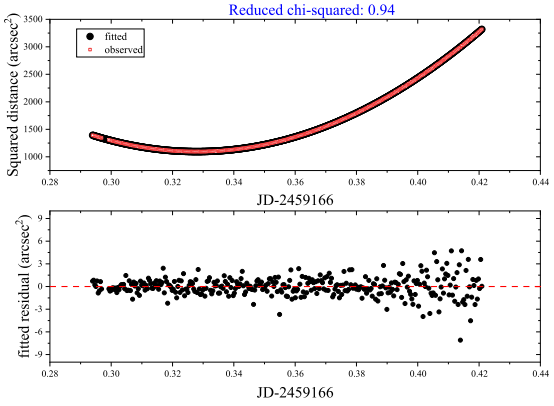

Figure A3. The figure shows the distance curve and fitted residuals of d^2 with time. The reference star ID is 190945110588179456, approached on 2020 November 12.

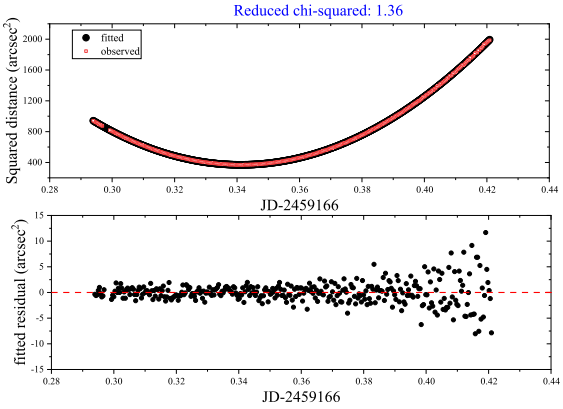

Figure A4. The figure shows the distance curve and fitted residuals of d^2 with time. The reference star ID is 190945106293176064, approached on 2020 November 12.

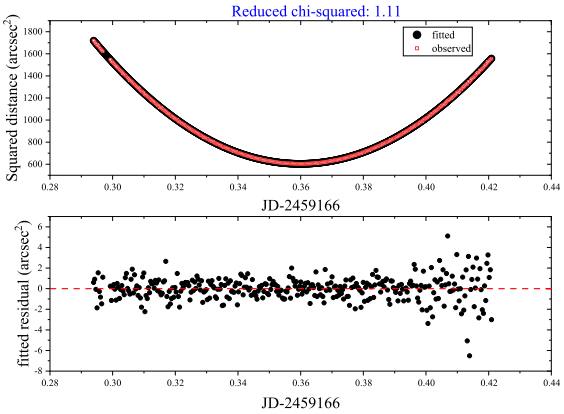

Figure A5. The figure shows the distance curve and fitted residuals of d^2 with time. The reference star ID is 190945316746612608, approached on 2020 November 12.

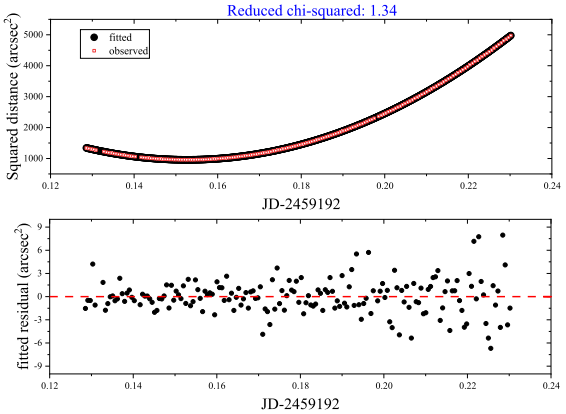

Figure A6. The figure shows the distance curve and fitted residuals of d^2 with time. The reference star ID is 188197534110556032, approached on 2020 December 8.

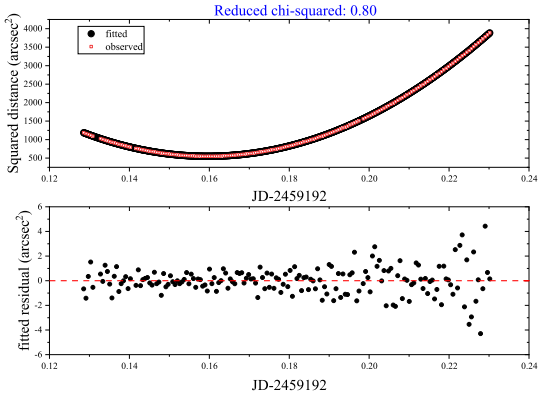

Figure A7. The figure shows the distance curve and fitted residuals of d^2 with time. The reference star ID is 188197534110557952, approached on 2020 December 8.

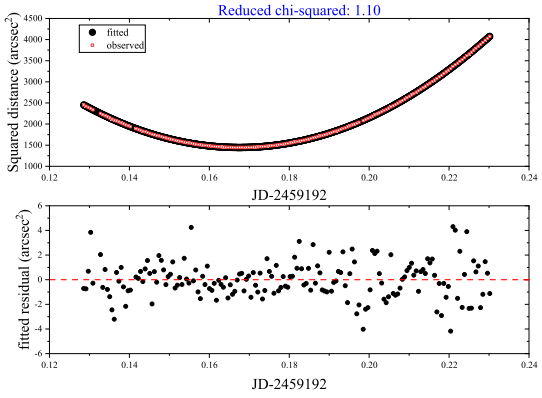

Figure A8. The figure shows the distance curve and fitted residuals of d^2 with time. The reference star ID is 188197534110557696, approached on 2020 December 8.

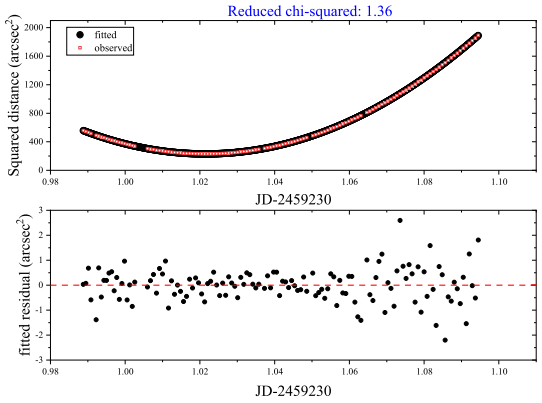

Figure A9. The figure shows the distance curve and fitted residuals of d^2 with time. The reference star ID is 173523550707799552, approached on 2021 January 15.

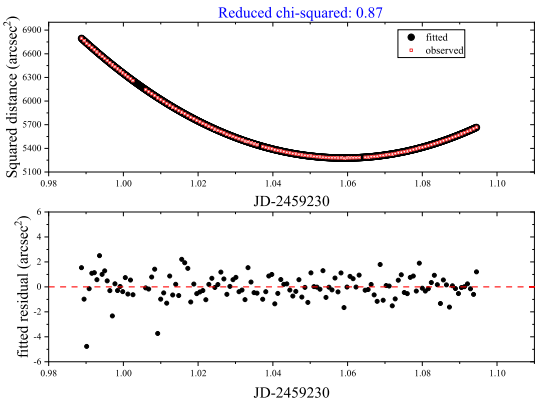

Figure A10. The figure shows the distance curve and fitted residuals of d^2 with time. The reference star ID is 173523275829562624, approached on 2021 January 15.

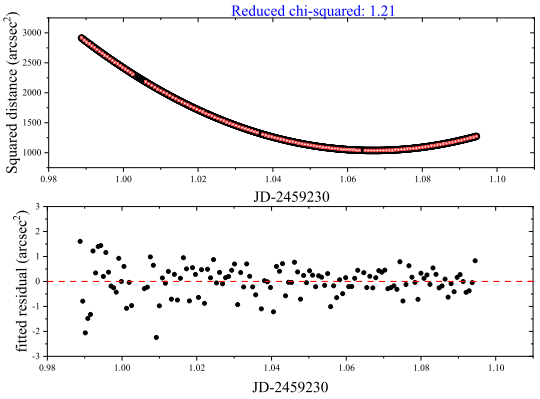

Figure A11. The figure shows the distance curve and fitted residuals of d^2 with time. The reference star ID is 173523344549362432, approached on 2021 January 15.

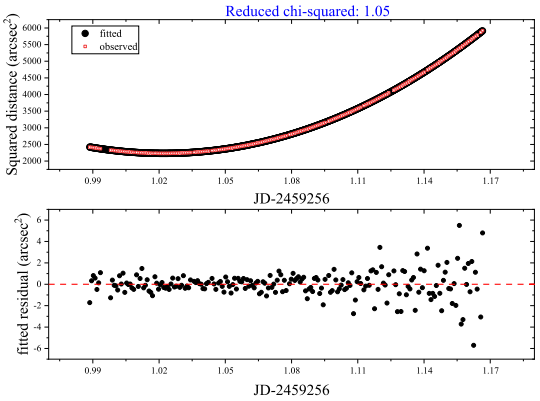

Figure A12. The figure shows the distance curve and fitted residuals of d^2 with time. The reference star ID is 159439940627025408, approached on 2021 February 10.

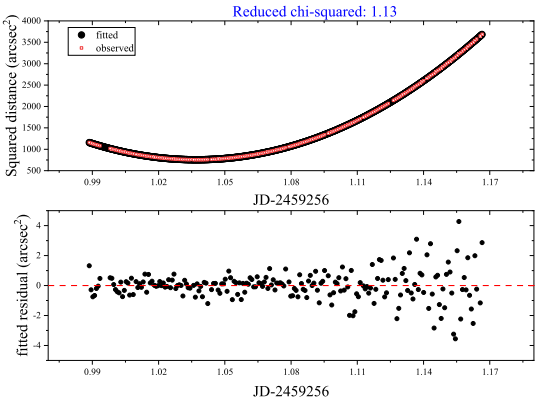

Figure A13. The figure shows the distance curve and fitted residuals of d^2 with time. The reference star ID is 159440048001339008, approached on 2021 February 10.

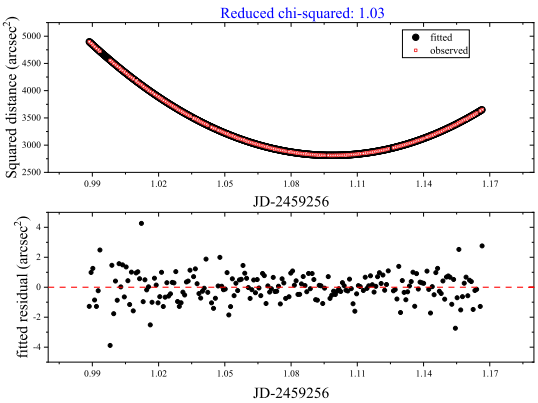

Figure A14. The figure shows the distance curve and fitted residuals of d^2 with time. The reference star ID is 159439910562389760, approached on 2021 February 10.

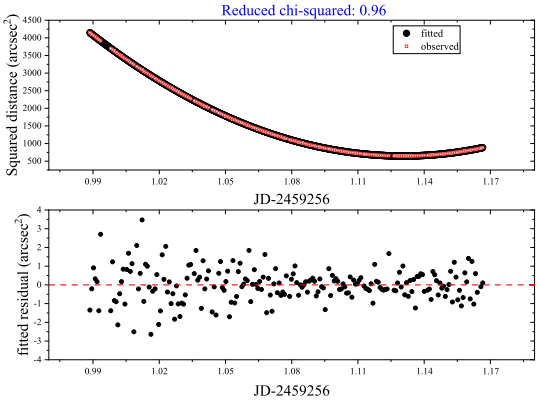

Figure A15. The figure shows the distance curve and fitted residuals of d^2 with time. The reference star ID is 159439738763696640, approached on 2021 February 10.

This paper has been typeset from a TEX/LATEX file prepared by the author.